Lateral Josephson effect on the surface of the magnetic Weyl semimetal $Co_3Sn_2S_2$

O. O. Shvetsov, V. D. Esin, Yu. S. Barash, A. V. Timonina, N. N. Kolesnikov, and E. V. Deviatov
Institute of Solid State Physics of the Russian Academy of Sciences, Moscow District, 2 Academician Ossipyan Str., Chernogolovka 142432, Russia

(Received 19 September 2019; revised manuscript received 9 January 2020; published 21 January 2020)

We experimentally study lateral electron transport between two 5-μm-spaced superconducting indium leads on a top of magnetic Weyl semimetal $Co_3Sn_2S_2$. For the disordered magnetic state of $Co_3Sn_2S_2$ crystal, we observe only the Andreev reflection in the proximity of each of the leads, which is indicative of highly transparent In-$Co_3Sn_2S_2$ interfaces. If the sample is homogeneously magnetized, it demonstrates a well-developed anomalous Hall effect state. In this regime we find the Josephson current that takes place even for 5-μm-long junctions and show the unusual magnetic field and temperature dependencies. As a possible reason for the results obtained, we discuss the contribution to the proximity-induced spin-triplet Josephson current from the topologically protected Fermi-arc states on the surface of $Co_3Sn_2S_2$.

DOI: 10.1103/PhysRevB.101.035304

I. INTRODUCTION

Similarly to topological insulators [1] and quantum Hall systems [2,3], Weyl semimetals [4,5] (WSM) have topologically protected surface states. They are Fermi arcs connecting projections of Weyl nodes on the surface Brillouin zone, and these surface states inherit the chiral property of the Chern insulator edge states [5]. WSMs should have either space-inversion or time-inversion symmetry to be broken. First, experimentally investigated WSMs were noncentrosymmetric crystals, where spin- and angle-resolved photoemission spectroscopy data have demonstrated spin-polarized surface Fermi arcs [6,7].

There are only a few candidates of magnetically ordered materials [4,8–10] for the realization of WSMs in systems with broken time-reversal symmetry. Recently, a giant anomalous Hall effect (AHE) was reported [11,12] for the kagome-lattice ferromagnet $Co_3Sn_2S_2$ as an anomalous Hall conductance in zero magnetic field. The AHE can be regarded as the indication to a magnetic Weyl phase [5], as supported by the topological-insulator-multilayer model, where the two-dimensional Chern edge states form the three-dimensional WSM surface states [13]. The Fermi-arc surface states, indeed, were directly visualized in $Co_3Sn_2S_2$ by scanning tunneling spectroscopy [14].

For normal metals, Andreev reflection [15] allows charge transport from the metal (N) to superconductor (S) through the NS interface by creating a Cooper pair at energies below the superconducting gap [15,16]. For two closely spaced superconducting leads, i.e., for the SNS junction, multiple Andreev reflections can contribute to the subharmonic structure of the current-voltage characteristics [16,17].

For topological materials, the proximity to a superconductor usually demonstrates nontrivial physics [18–20]. As it was experimentally shown, the Josephson coupling in a topological insulator is established through the surface conducting channels [21]. The edge current contribution can be retrieved even for systems with conducting bulk by analyzing the Josephson current behavior [22–24]. In Weyl semimetals, various topological superconducting states can appear [25–28] and various types of Andreev reflection can take place [28,29], depending on the particular conditions. Thus the specular Andreev reflection, reminiscent of the one in graphene [30,31], can take place at the Weyl semimetal–Weyl superconductor interface [29], while the chirality blockade of Andreev reflection can appear at the interface of the magnetic Weyl semimetal and the conventional *s*-wave spin-singlet superconductor [28].

For magnetically ordered topological materials the proximity to a superconductor is a new and emerging field involving the mutual influence of superconductivity and magnetism under nontrivial topological conditions, e.g., in the presence of topologically protected interface states. For example, it has been theoretically identified that the proximity to a superconductor can result in the Majorana modes originating from the Fermi arc in a Weyl semimetal wire with an axial magnetization [32]. It has also been predicted [33] that the proximity-induced superconducting surface states of magnetically doped topological insulators can represent chiral Majorana modes. Thus, it is reasonable to study proximity effects in superconducting junctions, fabricated on a three-dimensional magnetic Weyl semimetal surface.

Here, we experimentally study lateral electron transport between two 5-μm-spaced superconducting indium leads on a top of magnetic Weyl semimetal $Co_3Sn_2S_2$. For the disordered magnetic state of $Co_3Sn_2S_2$ crystal, we observe only the Andreev reflection in the proximity of each of the leads, which is indicative of highly transparent In-$Co_3Sn_2S_2$ interfaces. If the sample is homogeneously magnetized, it demonstrates a well-developed anomalous Hall effect state. In this regime we find the Josephson current that takes place even for 5-μm-long junctions and show the unusual magnetic field and temperature dependencies. As a possible reason for the results obtained, we discuss the contribution to the proximity-induced spin-triplet Josephson current from the topologically protected Fermi-arc states on the surface of $Co_3Sn_2S_2$.

 ©2020 American Physical Society

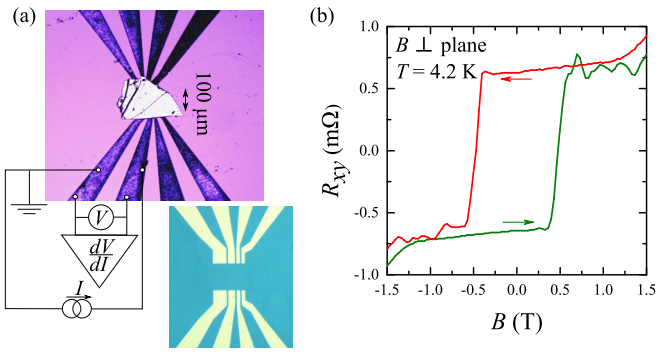

FIG. 1. (a) A top-view image of the sample with the sketch of electrical connections. A flat (about 100-μm size and 1-μm thick) single-crystal $Co_3Sn_2S_2$ flake is weakly pressed on the insulating SiO_2 substrate with 100-nm-thick, 5-μm separated In leads. The leads pattern is demonstrated in the bottom image. Nonlinear $dV/dI(I)$ curves are measured by a standard four-point technique, and all the wire resistances are excluded. (b) Giant anomalous Hall effect, which confirms the high quality of our $Co_3Sn_2S_2$ samples [11,12]. Arrows indicate the field scanning directions.

II. SAMPLES AND TECHNIQUE

$Co_3Sn_2S_2$ single crystals were grown by the gradient freezing method. An initial load of high-purity elements taken in stoichiometric ratio was slowly heated up to 920 °C in the horizontally positioned evacuated silica ampule, held for 20 h, and then cooled with the furnace to ambient temperature at the rate of 20 deg/h. The obtained ingot was cleaved in the middle part. The Laue patterns confirm the hexagonal structure with (0001) as a cleavage plane. Electron probe microanalysis of cleaved surfaces and x-ray diffractometry of powdered samples confirmed the stoichiometric composition of the crystal.

Weyl semimetals are essentially three-dimensional [5] macroscopic crystals. Despite that it is possible to form contacts directly on the polished crystal plane, we use another technique which is known to provide highly transparent contacts [20,24,34]. The leads pattern is formed on the insulating SiO_2 substrate by a lift-off technique after thermal evaporation of 100 nm In, see Fig. 1(a). The indium leads are separated by 5-μm intervals. Since the kagome-lattice ferromagnet $Co_3Sn_2S_2$ can be easily cleaved along the (0001) crystal plane, small (about 100 μm size and 1 μm thick) $Co_3Sn_2S_2$ flakes are obtained by a mechanical cleaving method. Then we select the most plane-parallel flakes with a clean surface, where no surface defects could be resolved with an optical microscope. They are transferred to the In leads pattern and pressed slightly with another oxidized silicon substrate. A special metallic frame allows us to keep the substrates parallel and apply a weak pressure to the sample. No external pressure is needed for a $Co_3Sn_2S_2$ flake to hold on to a substrate with In leads afterward. This procedure provides transparent contacts, stable in different cooling cycles, which has been also demonstrated before [20,24,34].

Magnetoresistance measurements confirms the high quality of the prepared $Co_3Sn_2S_2$ samples. We check that the samples demonstrate a giant anomalous Hall effect, as it has been previously reported [11,12], for $Co_3Sn_2S_2$ semimetal. Figure 1(b) shows hysteresis behavior and sharp switchings in Hall resistance R_{xy}, and the switching positions of ≈0.5 T quantitatively coincide with the reported values [11,12]. According to our sample dimensions, the Hall resistivity ρ_{xy} can be estimated as 1 $\mu\Omega$ cm in zero magnetic field, which is 3 times smaller in comparison with Refs. [11,12].

We study electron transport between two 5-μm separated In leads by a standard four-point technique. The principal circuit diagram is depicted in Fig. 1(a). In this connection scheme, all the wire resistances are excluded, which is necessary for low-impedance In-$Co_3Sn_2S_2$-In junctions. To obtain $dV/dI(I)$ characteristics, the dc current I (up to 1 mA) is additionally modulated by a low (≈5 μA) ac component. We measure both dc (V) and ac (the latter is proportional to dV/dI) components of the voltage drop with a dc voltmeter and a lock-in, respectively, after a broad-band preamplifier. The measurements are performed in a dilution refrigerator for the temperature interval 30 mK–1.2 K.

If the SNS junction demonstrates zero resistance, an important information can be obtained [22–24] from the maximum supercurrent I_c suppression by temperature T and magnetic field B. To obtain I_c values with high accuracy for given (B, T) values, we sweep current I ten times from zero value (superconducting $dV/dI = 0$ state) to some value well above the I_c value (i.e., to the resistive $dV/dI > 0$ state) and then determine I_c as an average value of $dV/dI = 0$ breakdown positions in different sweeps.

III. EXPERIMENTAL RESULTS

$Co_3Sn_2S_2$ magnetic properties arise from the kagome-lattice cobalt planes, whose magnetic moments order ferromagnetically [11] out of plane below 175 K. Since the samples are cooled down from room temperature in zero magnetic field, the initial state of a macroscopic $Co_3Sn_2S_2$ flake is a magnetically disordered one, e.g., due to magnetic domains. The size of these domains is typically around the order of a micrometer [35] in $Co_3Sn_2S_2$, which is much smaller than the distance between the indium leads in our samples. To obtain a definite AHE state of magnetically ordered WSM, the magnetization procedure is performed: an external magnetic field is swept slowly from −1.5 to +1.5 T, both limits being far above the switching positions in Fig. 1(b). Afterward, the external field goes down to zero.

Examples of $dV/dI(I)$ characteristics are shown in Figs. 2(a) and 2(b) before and after the magnetization procedure, respectively, for the same sample in a single cooling cycle.

Before magnetization, the curves demonstrate well-known Andreev behavior. Since Andreev reflection allows subgap transport of Cooper pairs, it appears experimentally as the resistance drop for voltages within the superconducting gap [16]. As it can be seen in Fig. 2(a), differential resistance is diminished within ≈ ± 0.5 mA bias interval with respect to the normal resistance value ≈0.5Ω. The superconducting gap can be estimated from the width of this region as 0.5 mA × 0.5 Ω ≈ 0.25 meV. Since the bulk indium is known [36] to have the 0.5-meV gap, the obtained value is quite reasonable for the indium film on a top of a ferromagnet. Temperature has low effect on $dV/dI(I)$ curves; even at 40 mK the minimal

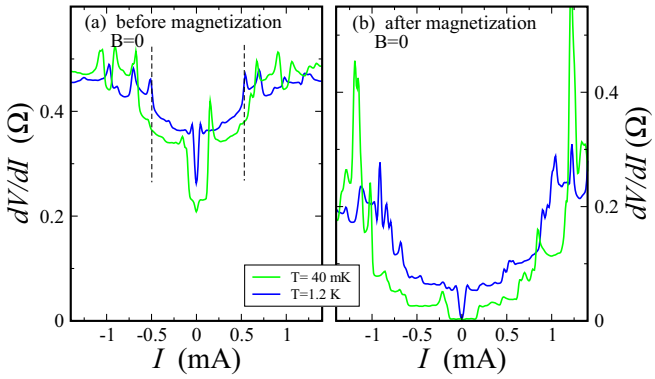

FIG. 2. Examples of $dV/dI(I)$ curves before sample magnetization (a) and after it (b), for the same sample in a single cooling cycle. Diminishing the temperature from 1.2 K to 40 mK has little effect on the initial Andreev-like $dV/dI(I)$ curves in (a). Dashed lines indicate the wide dV/dI resistance drop in (a), caused by Andreev reflection. In contrast, the magnetization procedure transforms $dV/dI(I)$ curves into the Josephson-like ones in (b). The width of a wide zero-resistance region depends on the temperature below 1.2 K. The data are obtained in zero magnetic field.

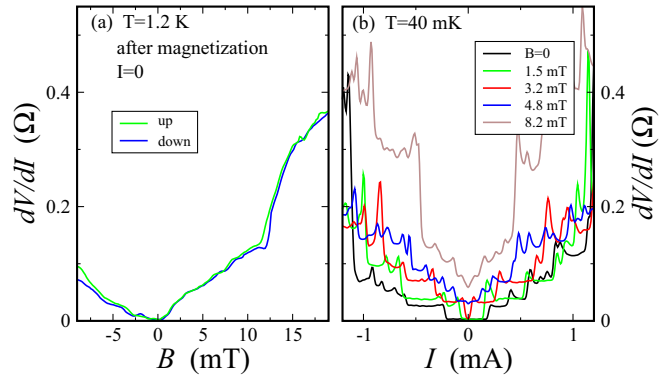

FIG. 3. Suppression of the zero-resistance state by magnetic field. (a) Differential resistance dV/dI at zero dc current as a function of magnetic field. A finite zero-resistance region can be seen even at the highest temperature, 1.2 K. Two curves correspond to the opposite field sweep directions and do not strictly coincide in the normal state. (b) Examples of $dV/dI(I)$ characteristics for different magnetic fields at 40 mK. The zero-resistance region survives above 3.2 mT at this temperature. The magnetic field is perpendicular to the flake's plane. The sample is the same as in Fig. 2 (after magnetization).

resistance is not below one-half of the normal value, see Fig. 2(a).

The magnetization procedure changes the $dV/dI(I)$ curves dramatically, see Fig. 2(b): the zero-bias resistance value drops to zero. At low temperature of 40 mK, we observe a definite zero-resistance state in a wide current region, which qualitatively resembles the Josephson effect [16]. This behavior has been checked to be independent of the value and sign of the magnetization field.

As it is expected for the Josephson effect, the zero-resistance state can be suppressed by magnetic field. Even at the highest temperature, the junction resistance is zero in a finite, ±1-mT field interval, see Fig. 3(a). This behavior is demonstrated in detail in Fig. 3(b) for $dV/dI(I)$ curves at lowest temperature of 40 mK. The zero-resistance state survives up to 3.2 mT. Above a 3.2-mT field, $dV/dI(I)$ curves demonstrate usual Andreev behavior, because the indium leads are still superconducting below the critical indium field [37] of about 40 mT.

Thus, we demonstrate in Figs. 2 and 3 that two superconducting contacts induce Josephson current in an unprecedentedly long $L = 5$ μm In-$Co_3Sn_2S_2$-In junction. The above-described behavior can be reproduced for different samples, see, e.g., Fig. 4. In this case, the normal dV/dI resistance is one order higher, about 3 Ohm, as depicted in the main field in Fig. 4(a). The differential resistance is diminished within a ±0.075-mA interval, which gives the same 0.075 mA× 3 Ω ≈ 0.25 meV superconducting gap value. Before sample magnetization, dV/dI is always finite even at 40 mK, see Fig. 4(a), while it drops to zero after the magnetization procedure.

We also observe unusual behavior of the temperature and magnetic field dependences of the critical current I_c. Lower currents are more suitable for accurate determination of I_c, so the results are presented in the insets to Figs. 4(a) and 4(b). All the experimental points are well reproducible; the variation of I_c in different sweeps is below the symbol size in the inset.

$I_c(T)$ demonstrates weak temperature dependence below 0.75 K, while I_c is diminishing strongly above it to one-half of the initial value at our highest 1.2 K, see the inset to Fig. 4(a). This dependence can be crudely extrapolated to ≈2 K critical temperature, which corresponds well to the

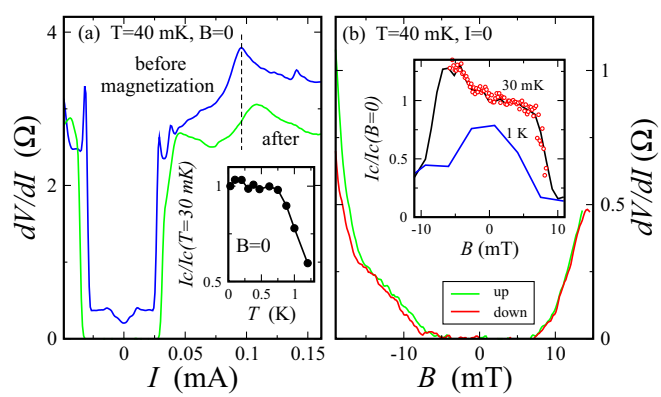

FIG. 4. Experimental results for a different sample at minimal 40-mK temperature. (a) Formation of the Josephson-type curve (the green one) with well-defined critical current (about 0.025 mA) after sample magnetization. Dashed line indicates the superconductive gap position for the Andreev-like curve (the blue one) without zero-resistance state. Inset demonstrates the temperature dependence of the critical current, which is unusual for long diffusive Josephson junctions. (b) Suppression of the zero-resistance state by magnetic field at zero dc current for two opposite field sweep directions. Inset demonstrates critical current as a function of magnetic field for two different temperatures. At 40 mK, the $I_c(B)$ is antisymmetric with respect to the zero field but symmetrically falls to zero at ±7 mT. The antisymmetry is confirmed by the extremely slow field sweep with a low step, as demonstrated by open circles. The expected $I_c(B)$ symmetry is restored above 1 K. The magnetic field is perpendicular to the flake's plane.

0.25-meV superconducting gap, determined from the Andreev curve in Fig. 4(a). However, $I_c(T)$ does not demonstrate the conventional for a long diffusive SNS junction exponential decay [38,39]. The experimental $I_c(T)$ resembles the results for Josephson junctions with spin-flip scattering [40].

The zero-resistance state at $I = 0$ is suppressed by magnetic field at ± 7 mT, see Fig. 4(b). The full $I_c(B)$ pattern is depicted in the inset to Fig. 4(b). At lowest temperatures, $I_c(B)$ is changing very slowly (within 10%) until ± 7 mT but falls to zero above this value. The characteristic feature is that the low-field $I_c(B)$ dependence is antisymmetric with respect to the zero field. This behavior is confirmed by an extremely slow field sweep with a large amount of points, as demonstrated by open circles in the inset. There are also some $I_c(B)$ oscillations within the ± 7-mT interval. Both the antisymmetry and the oscillations are destroyed by temperature above 0.75 K. The shallow oscillations in $I_c(B)$ could be related with usual interference effects [16], although the corresponding curve substantially differs from the standard Fraunhofer pattern [41] and no strong suppression of $I_c(B)$ at $B < \pm 7$ mT is observed.

It is important that both for the resistance at $I = 0$ in the main Fig. 4(b) and for significant current $\approx$0.05 mA in the inset, the Josephson effect is destroyed under the same magnetic fields, ± 7 mT. Thus, there is no sample overheat in $I_c(B, T)$ measurements, so the unusual $I_c(T)$ temperature dependence is correct in the inset to Fig. 4(a).

IV. DISCUSSION

As a result, we demonstrate Josephson current through the magnetically ordered 5-μm-long In-$Co_3Sn_2S_2$-In junctions, where the $Co_3Sn_2S_2$ flake is in a definite AHE state. On the other hand, no supercurrent can be observed in these junctions when $Co_3Sn_2S_2$ is in the disordered magnetic state. This effect is well reproducible for different samples, see Figs. 2 and 4(a).

First of all, we should exclude possible fabrication defects such as unintentional shunt connections in the junction's plane. The crucial argument against the presence of any leakage is a pronounced dependence of the Josephson effect on the WSM magnetization. For conventional superconductors like indium, the proximity to a ferromagnet weakens superconductivity. Just opposite to the known indium behavior, the magnetically ordered state of $Co_3Sn_2S_2$ enhances the Josephson coupling. Also, the thickness of the indium film is chosen to be much smaller than the lead separation (100 nm $<<$ 5 μm) to avoid shorting of In leads when pressing the $Co_3Sn_2S_2$ flake. Thus, one can be sure that the observed Josephson current flows through the proximity-influenced magnetically ordered $Co_3Sn_2S_2$ WSM.

The surface-state transport can be a key point to explain our experimental results. In the case of $Co_3Sn_2S_2$, Fermi-arc surface states have been directly identified by scanning tunneling spectroscopy [14]. The giant anomalous Hall effect is interpreted in terms of the surface states [5], and we observe the Josephson effect only after the magnetization procedure, i.e., for a well-pronounced AHE state, see Fig. 1(b). Therefore, Weyl surface states exist along the macroscopic $Co_3Sn_2S_2$ flake. Their proximity-induced pairing results in the effective supercurrent-carrying channels. The important role of the chiral surface channels in the Josephson transport studied is also supported by their topological protection and the lateral geometry of the junction.

The magnetic domain structure in the $Co_3Sn_2S_2$ flake can have a substantial influence on the junction's properties. When the domain magnetization in the $Co_3Sn_2S_2$ sample is disordered just after the sample cooling, the chirality of Weyl nodes can switch across the magnetic domain walls [5] and a continuous surface state can appear only along a single magnetic domain, the size being around the order of a micrometer [35]. Such a disordered magnetic structure should produce significant disordered spin-flip processes and can prevent the Josephson effect to develop between the 5-μm-spaced indium leads, allowing only the observation of Andreev reflection in the proximity of each of the leads, in accordance with our measurements for samples before the magnetization procedure.

Since the Weyl surface states are spin polarized [5,14,42] and $Co_3Sn_2S_2$ itself is a half-metal [42], one can expect a triplet supercurrent [43–45] through $Co_3Sn_2S_2$. When singlet Cooper pairs from the superconductor are converted into triplet pairs within the spin-polarized material, a long-range proximity effect, as known, can take place: while the singlet component penetrates into the ferromagnet over a short length [46] $\xi_h = (\hbar D/E_{\rm ex})^{1/2}$($E_{\rm ex}$ is the exchange energy and D is the diffusion coefficient), the triplet component penetrates over a much longer length $(\hbar D/k_B T)^{1/2}$, which is of the same order as that for the penetration of the superconducting pairs into a normal metal [43]. This conclusion prohibits, in particular, the conventional long-range s-wave spin-singlet pairing in a $Co_3Sn_2S_2$ flake, which occurs in In and cannot be present in the magnetic Weyl semimetal, as also follows from the chirality blockade arguments [28]. Since the exchange field and spin-orbit coupling are jointly present in Weyl semimetals, the singlet-triplet conversion at its interface does not require additional magnetic inhomogeneities [47,48].

The triplet supercurrent can be responsible for the low-field $I_c(B)$ antisymmetry in the inset to Fig. 4(b). While in topological insulators the surface-conducting channels have been experimentally identified as dominating in establishing the Josephson coupling [21], the Josephson current in Weyl semimetals can be transferred generally via both the surface and the bulk channels [49]. The low-field variation of $I_c(B)$ reflects the magnetization dynamics in the bulk $Co_3Sn_2S_2$, since in the inset to Fig. 4(b) I_c is smaller for positive fields and for a positively magnetized flake. As opposed to the low-field region, the fields exceeding $B_c \approx \pm 7$ mT can be considered as destroying the superconducting pairing via the surface channels, where the topologically protected magnetic ordering is not sensitive to the lower values of the external field. We wish to mention that uneven indium contact spacing may distort the behavior of $I_c(B)$; for example, it (partly) suppresses the Fraunhofer pattern [41]. However, it cannot make $I_c(B)$ become sensitive to the sign of the magnetic field, which we observe as the low-field antisymmetry.

V. CONCLUSION

As a conclusion, we experimentally study lateral electron transport between two 5-μm-spaced superconducting indium

leads on a top of magnetic Weyl semimetal $Co_3Sn_2S_2$. For the disordered magnetic state of $Co_3Sn_2S_2$ crystal, we observe only the Andreev reflection in the proximity of each of the leads, which is indicative of highly transparent In-$Co_3Sn_2S_2$ interfaces. If the sample is homogeneously magnetized, it demonstrates a well-developed anomalous Hall effect state. In this regime we find the Josephson current that takes place even for 5-μm-long junctions and shows the unusual magnetic field and temperature dependencies. As a possible reason for the results obtained, we discuss the contribution to the proximity-induced spin-triplet Josephson current from the topologically protected Fermi-arc states on the surface of $Co_3Sn_2S_2$.

ACKNOWLEDGMENTS

We wish to thank V. T. Dolgopolov for fruitful discussions and S. V. Simonov for x-ray sample characterization. We gratefully acknowledge financial support partially by the RFBR (Project No. 19-02-00203), RAS, and RF State tasks.

[1] M. Z. Hasan and C. L. Kane, Rev. Mod. Phys. **82**, 3045 (2010).
[2] M. Büttiker, Phys. Rev. B **38**, 9375 (1988).
[3] E. V. Deviatov, Phys.-Usp. **50**, 197 (2007).
[4] X. Wan, A. M. Turner, A. Vishwanath, and S. Y. Savrasov, Phys. Rev. B **83**, 205101 (2011).
[5] For a review on topological semimetals, see N. P. Armitage, E. J. Mele, and A. Vishwanath, Rev. Mod. Phys. **90**, 015001 (2018).
[6] P. K. Das, D. D. Sante, I. Vobornik, J. Fujii, T. Okuda, E. Bruyer, A. Gyenis, B. E. Feldman, J. Tao, R. Ciancio, G. Rossi, M. N. Ali, S. Picozzi, A. Yadzani, G. Panaccione, and R. J. Cava, Nat. Commun. **7**, 10847 (2016).
[7] B. Feng, Y.-H. Chan, Y. Feng, R.-Y. Liu, M.-Y. Chou, K. Kuroda, K. Yaji, A. Harasawa, P. Moras, A. Barinov, W. Malaeb, C. Bareille, T. Kondo, S. Shin, F. Komori, T.-C. Chiang, Y. Shi, and I. Matsuda, Phys. Rev. B **94**, 195134 (2016).
[8] M. Hirschberger, S. Kushwaha, Z. Wang, Q. Gibson, S. Liang, C. A. Belvin, B. A. Bernevig, R. J. Cava, and N. P. Ong, Nat. Mater. **15**, 1161 (2016).
[9] G. Xu, H. Weng, Z. Wang, X. Dai, and Z. Fang, Phys. Rev. Lett. **107**, 186806 (2011).
[10] S. K. Kushwaha, Z. Wang, T. Kong, and R. J. Cava, J. Phys.: Condens. Matter. **30**, 075701 (2018).
[11] E. Liu, Y. Sun, N. Kumar, L. Muechler, A. Sun, L. Jiao, S.-Y. Yang, D. Liu, A. Liang, Q. Xu *et al.*, Nat. Phys. **14**, 1125 (2018).
[12] Q. Wang, Y. Xu, R. Lou, Z. Liu, M. Li, Y. Huang, D. Shen, H. Weng, S. Wang, and H. Lei, Nat. Commun. **9**, 3681 (2018).
[13] A. A. Burkov and L. Balents, Phys. Rev. Lett. **107**, 127205 (2011).
[14] N. Morali, R. Batabyal, P. K. Nag, E. Liu, Q. Xu, Y. Sun, B. Yan, C. Felser, N. Avraham, and H. Beidenkopf, Science **365**, 1286 (2019).
[15] A. F. Andreev, Sov. Phys. JETP **19**, 1228 (1964).
[16] M. Tinkham, *Introduction to Superconductivity*, 2nd ed. (McGrawHill, New York, 1996).
[17] N. Agrait, A. Levy Yeyati, and J. M. van Ruitenbeek, Phys. Rep. **377**, 81 (2003).
[18] L. Fu and C. L. Kane, Phys. Rev. Lett. **100**, 096407 (2008).
[19] A. Kononov, V. A. Kostarev, B. R. Semyagin, V. V. Preobrazhenskii, M. A. Putyato, E. A. Emelyanov, and E. V. Deviatov, Phys. Rev. B **96**, 245304 (2017).
[20] A. Kononov, O. O. Shvetsov, S. V. Egorov, A. V. Timonina, N. N. Kolesnikov, and E. V. Deviatov, Europhys. Lett. **122**, 27004 (2018).
[21] J. H. Lee, G.-H. Lee, J. Park, J. Lee, S.-G. Nam, Y.-S. Shin, J. S. Kim, and H.-J. Lee, Nano Lett. **14**, 5029 (2014).
[22] S. Hart, H. Ren, T. Wagner, P. Leubner, M. Mühlbauer, C. Brüne, H. Buhmann, L. W. Molenkamp, and A. Yacoby, Nat. Phys. **10**, 638 (2014).
[23] V. S. Pribiag, A. J. A. Beukman, F. Qu, M. C. Cassidy, C. Charpentier, W. Wegscheider, and L. P. Kouwenhoven, Nat. Nanotechnol. **10**, 593 (2015).
[24] O. O. Shvetsov, A. Kononov, A. V. Timonina, N. N. Kolesnikov, and E. V. Deviatov, JETP Lett. **107**, 774 (2018); Europhys. Lett. **124**, 47003 (2018).
[25] T. Meng and L. Balents, Phys. Rev. B **86**, 054504 (2012).
[26] G. Y. Cho, J. H. Bardarson, Y.-M. Lu, and J. E. Moore, Phys. Rev. B **86**, 214514 (2012).
[27] H. Wei, S. P. Chao, and V. Aji, Phys. Rev. B **89**, 014506 (2014).
[28] N. Bovenzi, M. Breitkreiz, P. Baireuther, T. E. O'Brien, J. Tworzydło, İ. Adagideli, and C. W. J. Beenakker, Phys. Rev. B **96**, 035437 (2017).
[29] W. Chen, L. Jiang, R. Shen, L. Sheng, B. G. Wang, and D. Y. Xing, Europhys. Lett. **103**, 27006 (2013).
[30] C. W. J. Beenakker, Phys. Rev. Lett. **97**, 067007 (2006).
[31] C. W. J. Beenakker, Rev. Mod. Phys. **80**, 1337 (2008).
[32] P. Baireuther, J. Tworzydlo, M. Breitkreiz, I. Adagideli, and C. W. J. Beenakker, New J. Phys. **19**, 025006 (2017).
[33] T. Toki, S. Nakosai, Y. Tanaka, and Y. Kawaguchi, Phys. Rev. B **100**, 104518 (2019).
[34] O. O. Shvetsov, V. D. Esin, A. V. Timonina, N. N. Kolesnikov, and E. V. Deviatov, Phys. Rev. B **99**, 125305 (2019).
[35] Q. Xu, E. Liu, W. Shi, L. Muechler, J. Gayles, C. Felser, and Y. Sun, Phys. Rev. B **97**, 235416 (2018).
[36] A. M. Toxen, Phys. Rev. **123**, 442 (1961).
[37] P. Scharnhorst, Phys. Rev. B **1**, 4295 (1970).
[38] I. O. Kulik, Sov. Phys. JETP **30**, 944 (1970).
[39] P. Dubos, H. Courtois, B. Pannetier, F. K. Wilhelm, A. D. Zaikin, and G. Schön, Phys. Rev. B **63**, 064502 (2001).
[40] J. C. Hammer, J. C. Cuevas, F. S. Bergeret, and W. Belzig, Phys. Rev. B **76**, 064514 (2007).

[41] A. Barone and G. Paterno, *Physics and Applications of the Josephson Effect* (John Wiley & Sons, New York, 1982).
[42] L. Jiao, Q. Xu, Y. Cheon, Y. Sun, C. Felser, E. Liu, and S. Wirth, Phys. Rev. B **99**, 245158 (2019).
[43] F. S. Bergeret, A. F. Volkov, and K. B. Efetov, Phys. Rev. Lett. **86**, 4096 (2001).
[44] F. S. Bergeret, A. F. Volkov, and K. B. Efetov, Rev. Mod. Phys. **77**, 1321 (2005).
[45] R. S. Keizer, S. T. B. Goennenwein, T. M. Klapwijk, G. Miao, G. Xiao, and A. Gupta, Nature (London) **439**, 825 (2006).
[46] A. I. Buzdin, Rev. Mod. Phys. **77**, 935 (2005).
[47] F. S. Bergeret and I. V. Tokatly, Phys. Rev. Lett. **110**, 117003 (2013).
[48] F. S. Bergeret and I. V. Tokatly, Phys. Rev. B **89**, 134517 (2014).
[49] P. Dutta, F. Parhizgar, and A. M. Black-Schaffer, arXiv:1911.04388